Acta Crystallographica Section F
Structural Biology and Crystallization Communications
ISSN 1744-3091

There is a baby in the bath water: AcrB contamination is a major problem in membrane-protein crystallization

David Veesler,* Stéphanie Blangy, Christian Cambillau and Giuliano Sciara

Architecture et Fonction des Macromolécules Biologiques, CNRS et Universités d'Aix-Marseille I et II, UMR 6098, Case 932, 163 Avenue de Luminy, 13288 Marseille CEDEX 9, France

Correspondence e-mail: david.veesler@afmb.univ-mrs.fr

Received 12 June 2008
Accepted 3 September 2008

PDB Reference: AcrB, 3d9b, r3d9bsf.

In the course of a crystallographic study of the *Methanosarcina mazei* CorA transporter, the membrane protein was obtained with at least 95% purity and was submitted to crystallization trials. Small crystals (<100 µm) were grown that diffracted to 3.42 Å resolution and belonged to space group *R*32, with unit-cell parameters $a = b = 145.74$, $c = 514.0$ Å. After molecular-replacement attempts using available CorA structures as search models failed to yield a solution, it was discovered that the crystals consisted of an *Escherichia coli* contaminating protein, acriflavine resistance protein B (AcrB), that was present at less than 5% in the protein preparations. AcrB contamination is a major problem when expressing membrane proteins in *E. coli* since it binds naturally to immobilized metal-ion affinity chromatography (IMAC) resins. Here, the structure is compared with previously deposited AcrB structures and strategies are proposed to avoid this contamination.

1. Introduction

In the last few years, the number of membrane-protein structures deposited in the Protein Data Bank (PDB) has increased exponentially. Many of these proteins were heterologously overexpressed in *Escherichia coli* with a polyhistidine fusion tag for subsequent purification. Two well known critical factors in protein crystallization are protein purity and monodispersity. In the case of soluble proteins, reports can be found concerning the unfortunate crystallization of contaminating proteins either from a very low amount of contamination of the purified protein sample (Cámara-Artigas *et al.*, 2006) or even from a mixture of 50 different proteins with no predominant species (Lohkamp & Dobritzsch, 2008). In the case of membrane proteins, no report dedicated to the exposition of such situations has been previously published.

The CorA transport protein is the primary Mg^{2+}-uptake system in both bacteria and archaea. Thus, it is a key component of Mg^{2+} homeostasis in these kingdoms (Kehres & Maguire, 2002; Knoop *et al.*, 2005). Recently, three different groups have independently solved the structure of the pentameric *Thermotoga maritima* CorA, which is believed to be in a closed state (Lunin *et al.*, 2006; Eshaghi *et al.*, 2006; Payandeh & Pai, 2006). These structures, as well as a more recent report (Payandeh *et al.*, 2008), provide new insights into CorA transporters; however, the mechanism of pore opening and magnesium transport remains to be elucidated. Thus, the structure of CorA in the open state would be of great benefit in order to further understand this fascinating protein family.

During our attempts to crystallize a ligand-free archaeal homologue of CorA, we obtained crystals of an unexpected protein: AcrB from *E. coli*. This is a proton motive force-dependent multidrug efflux pump that functions *via* a drug/proton antiport mechanism and belongs to the resistance–nodulation–division (RND) transporter superfamily. It accepts substrates either from the periplasm or from the cytoplasm (Helling *et al.*, 2002) and works within a tripartite system involving an outer membrane channel (TolC) and a membrane-fusion protein (AcrA). AcrB spontaneously binds to IMAC resins because of the presence of a histidine-rich cluster at its

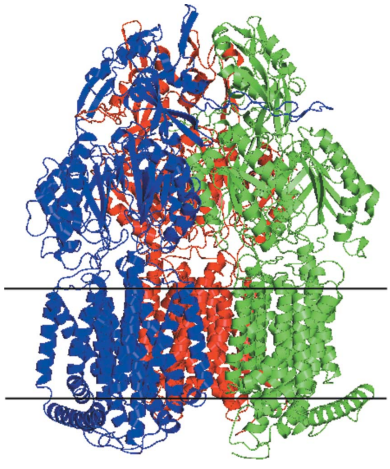

Table 1
Crystallographic data processing.

Values in parentheses are for the highest resolution shell.

Resolution range (Å)	20–3.42 (3.6–3.42)
Total observations	176182 (25406)
Unique observations	28788 (4072)
Completeness (%)	99.3 (100)
$R_{\rm merge}$† (%)	12.4 (61.9)
Multiplicity	6.12 (6.24)
$I/\sigma(I)$	11.97 (3.25)

† $R_{\rm merge} = \sum_{hkl}\sum_i |I_i(hkl) - \langle I(hkl)\rangle| / \sum_{hkl}\sum_i I_i(hkl)$.

C-terminus. Here, we describe a phenomenon that is very frequent in membrane-protein crystallography laboratories but that has been little documented in the literature. In addition, we present the structure of *E. coli* AcrB at 3.42 Å resolution from rhombohedral crystals.

2. Materials and methods

2.1. Cloning and expression

The genomic DNA sequence of *Methanosarcina mazei* CorA was amplified by PCR using specific Gateway primers containing *attB* sequences, which allow insertion into the pDONR201 cloning vector by the BP recombination reaction, and then introduced into a Gateway home-adapted pET22b vector (Novagen). The resulting construct (pET22b-CorA) bears a C-terminal His_6 tag. For protein expression, *E. coli* BL21 (DE3) strain (Invitrogen) was transformed with pET22b-CorA and cells were grown in a 3 l fermenter at 310 K with batch medium (Xu *et al.*, 1999) supplemented with 100 µg ml^{-1} ampicillin. When the OD_{600} reached 2.5, the temperature was reduced to 293 K and expression was induced overnight by the addition of 0.5 m*M* IPTG. Cells were harvested by centrifugation and stored at 193 K.

2.2. Purification

All steps were conducted at 277 K. Cells were resuspended in lysis buffer [50 m*M* Tris pH 8.0, 300 m*M* NaCl, 5%(*v*/*v*) glycerol, 1 m*M* EDTA, 0.5 mg ml^{-1} lysozyme, 20 µg ml^{-1} DNAse I, 20 m*M* $MgSO_4$, phenylmethylsulfonyl fluoride (PMSF) and antiproteases (Complete EDTA-free antiproteases, Roche)] and lysed by three passages through a French press (Thermo) at 124 MPa. Two low-speed centrifugation steps removed cellular debris, inclusion bodies and precipitated proteins. The resulting supernatant was ultracentrifuged in a Ti-45 rotor (Beckman-Coulter) at 40 000 rev min^{-1} for 1.5 h. The pellet (membranes) was resuspended in buffer *A* [50 m*M* Tris pH 8.0, 300 m*M* NaCl, 5%(*v*/*v*) glycerol, PMSF and antiproteases (Roche)], flash-frozen in liquid nitrogen and stored at 193 K. Solubilization of CorA was accomplished by stirring for 30 min in buffer *A* + 1% *n*-dodecyl-*β*-D-maltopyranoside (DDM; Solgrade, Anatrace) before ultracentrifugation at 40 000 rev min^{-1} for 1.5 h. The supernatant was then incubated with agitation for 30 min with 15 ml Ni–NTA resin (Qiagen) equilibrated in buffer *A* + 0.05% DDM (Solgrade, Anatrace). Washing and elution steps took place on a gravity column with buffer *A* + 0.05% DDM (Anagrade, Anatrace) containing 50 and 250 m*M* imidazole, respectively. CorA-containing fractions were pooled based on SDS–PAGE analysis. The protein was then injected onto a Superdex 200 16/60 column (Amersham) and run in a buffer containing 10 m*M* Tris pH 8.0, 300 m*M* NaCl, 5%(*v*/*v*) glycerol and 0.05% DDM (Anagrade, Anatrace). Two peaks were observed: the first was in the void volume (aggregated CorA) and the second corresponded to the pentameric form of CorA. Fractions from the second peak were pooled and concentrated to 6 mg ml^{-1} using a centrifugal filter device (Millipore, 100 kDa molecular-weight cutoff). Before crystallogenesis, the protein was ultracentrifuged in a Ti-42.2 rotor (Beckman-Coulter) at 42 000 rev min^{-1} for 30 min. Protein purity and integrity were checked by Coomassie-stained SDS–PAGE. The single observed band was excised for protease treatment. Protein digestion with trypsin took place as described previously (Shevchenko *et al.*, 1996) before peptide mass-fingerprint MALDI–TOF (PMF–MALDI–TOF) mass-spectrometric analysis. In all mass-spectrometric studies, spectra were acquired with an Autoflex spectrometer (Bruker Daltonics).

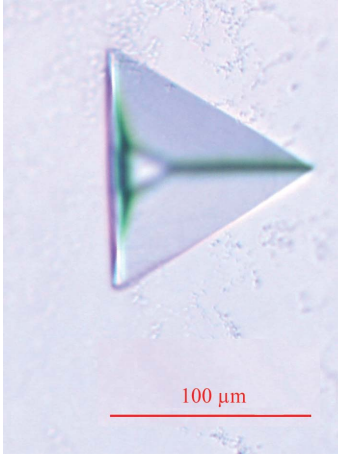

Figure 1
Rhombohedral crystal of *E. coli* AcrB.

2.3. Crystallization

Crystallization screening was performed using a sitting-drop vapour-diffusion setup in 96-well plates at 293 K. Initial hits were obtained with the commercial screens Membrane Class I and II (Qiagen). A lead condition (0.1 *M* MES pH 6.5, 30% PEG 400) was optimized in 24-well plates with 0.5 ml of precipitant solution in the reservoir to a range of final crystallization conditions: 0.1 *M* MES pH 6.0–7.0, 20–40% PEG 400. By varying the pH, the temperature, the protein and precipitant concentrations, the drop size and the protein:precipitant solution ratio, the best condition was found to be 3 µl protein solution + 2 µl mother liquor (0.1 *M* MES pH 6.6, 31% PEG 400). Crystals appeared after 10 d and reached maximum dimensions of 95 × 80 × 40 µm within about two months (Fig. 1). To improve crystal quality, various detergents were added to the reservoir solution. Most of those with a glucoside or a maltoside headgroup produced similar but significantly smaller crystals. However, the addition of 0.1% *n*-octyl-*β*-D-thioglucopyranoside (Anagrade, Anatrace) allowed us to obtain crystals as large as those obtained in DDM, but with a dramatic loss of diffraction power. For cryocooling, crystals were directly flash-frozen in a stream of boiling nitrogen.

2.4. Data collection and processing

Diffraction data were collected at the European Synchrotron Radiation Facility (Grenoble, France) on beamline ID-23 EH1 with a beam size of 100 × 100 µm using an ADSC Quantum Q315r detector. The sample temperature was 100 K and the wavelength was 0.98 Å. Each frame was taken with an oscillation of 1° and 1 s exposure at 10% transmission. Data from 100 images were indexed and integrated with *XDS* and scaled with *XSCALE* (Kabsch, 1993). The

AcrB crystals diffracted to 3.42 Å resolution and belonged to the rhombohedral space group $R32$, with unit-cell parameters $a = b = 145.74$, $c = 514.0$ Å. The calculated solvent content with one AcrB molecule in the asymmetric unit was 73.73% (V_M = 4.72 Å^3 Da^{-1}). A random selection of 4% of the data (test set) were assigned for calculation of the free R factor (Brünger, 1992) and were not included in the refinement. Data-collection and processing statistics are reported in Table 1.

2.5. Molecular-replacement attempts with CorA

The reported full-length structures of *T. maritima* CorA and the two soluble-domain structures of *T. maritima* and *Archaeoglobus fulgidus* CorA were used as molecular-replacement search models (PDB codes 2hn2, 2bbj, 2iub, 2hn1 and 2bbh). Unmodified and polyalanine models as well as various truncated structures based on these PDB entries were produced to generate potentially invariable search models. Attempts to solve the *M. mazei* CorA structure were made using *MOLREP* (Vagin & Teplyakov, 1997), *Phaser* (McCoy *et al.*, 2007), *FSEARCH* (Hao, 2001) and *RSEARCH* (Collaborative Computational Project, Number 4, 1994) using several resolution cutoffs. Moreover, we generated models predicting putative motions of CorA by normal-mode analysis of the full length, the transmembrane pore and the pentameric soluble domain of the *T. maritima* CorA structure (PDB code 2iub) using the *elNémo* server (Suhre & Sanejouand, 2004).

2.6. AcrB structure determination and refinement

We finally used the structure of *E. coli* AcrB solved at 3.1 Å resolution (PDB code 2i6w) without modification as the molecular-replacement search model for phasing with *MOLREP*. Refinement was carried out with *REFMAC*5 (Murshudov *et al.*, 1997) and model building was performed using *Coot* (Emsley & Cowtan, 2004). TLS groups were generated with the *TLS Motion Determination* server (Painter & Merritt, 2006). The structure was refined to R_{cryst} and R_{free} factors of 28.8% and 35.4%, respectively. The final AcrB model contained 1045 amino-acid residues and did not include the last four residues (1046–1049). Refinement and model validation statistics are reported in Table 2.

Table 2
Crystallographic refinement and model-validation statistics.

Values in parentheses are for the highest resolution shell.

Resolution range	20–3.42 (3.51–3.42)
No. of reflections used in refinement	27636 (1961)
Final overall R factor (%)	28.8 (34.1)
Atomic displacement model	Isotropic
Overall average B factor excluding solvent (Å^2)	67.7
No. of atoms	7951
No. of reflections in test set for R_{free}	1152 (82)
Final R_{free} (%)	35.4 (39.4)
R.m.s.d. deviation from ideal values	
R.m.s.d. bond lengths (Å)	0.01
R.m.s.d. bond angles (°)	1.40
R.m.s.d. dihedral angles (°)	1.19
Ramachandran plot analysis (excluding Gly and Pro)	
Most favoured (%)	82.8
Additional allowed (%)	15.4
Generously allowed (%)	1.4
Disallowed (%)	0.4

3. Results and discussion

3.1. CorA purity analysis

Classical Coomassie-stained SDS–PAGE analysis of the two-step purified CorA showed only one band at the expected molecular weight for the CorA monomer (46.9 kDa, Fig. 2*a*). PMF–MALDI–TOF mass spectrometry was used to unambiguously identify the protein in the unique observed band as *M. mazei* CorA (Fig. 2*b*).

3.2. AcrB identification

Before contamination was detected, we performed extensive molecular-replacement trials using CorA-based search models without success, despite the 46% sequence identity between *T. maritima* and *M. mazei* CorA. We were able to identify that the crystallized protein was *E. coli* AcrB instead of *M. mazei* CorA thanks to the helpful suggestions of Dr Liz Carpenter (Membrane Protein Laboratory, Diamond, Oxford, United Kingdom) and Dr Susanna Törnroth-Horsefield (University of Gothenburg, Sweden). The crystal morphology, space group and unit-cell parameters were typical of *E. coli* AcrB rhombohedral crystals.

E. coli AcrB spontaneously binds to IMAC resins because of the presence of a histidine-rich cluster at its C-terminus. Because of the low amount of contamination, the presence of AcrB was not detected by classical Coomassie-stained SDS–PAGE. Furthermore, MALDI–TOF mass spectrometry carried out on dissolved crystals did not allow us to observe AcrB. We estimated the AcrB concentration in our sample to be approximately 0.1 mg ml^{-1}.

3.3. AcrB crystallization conditions summary

We crystallized *E. coli* AcrB in a previously unreported condition using only PEG 400 as the precipitating agent. A summary of the crystallization conditions, crystal space groups and unit-cell para-

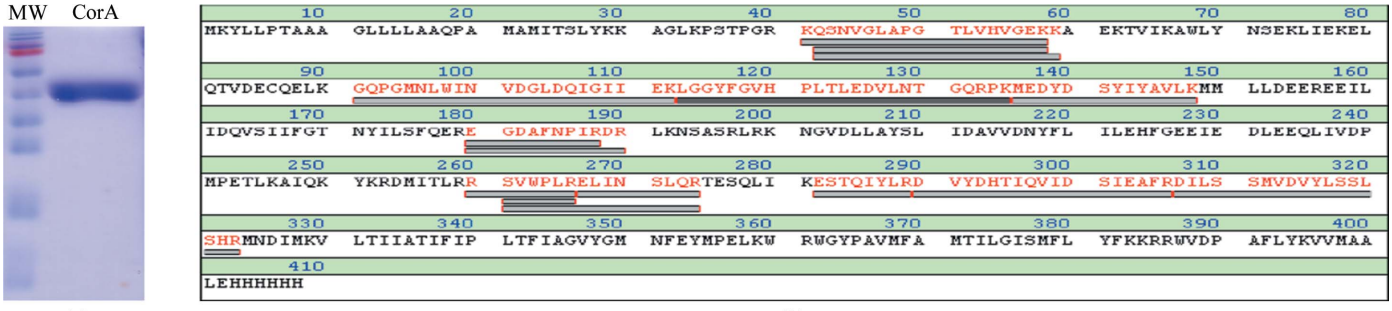

Figure 2
CorA purification. (*a*) Coomassie-stained SDS–PAGE of purified *M. mazei* CorA. Lane MW, molecular-weight markers (170, 130, 100, 70, 55, 40, 35, 25, 15 and 10 kDa); lane CorA, two-step purified *M. mazei* CorA. (*b*) Peptide mass-fingerprint MALDI–TOF identification using the sequence of *M. mazei* CorA and the band shown in Fig. 2(*a*). The sequence coverage was 35.5%. Grey bars indicate matching peptides.

Table 3
Summary of crystallization conditions for the 25 structures of *E. coli* AcrB deposited to date in the PDB.

For each structure, the crystal space group, unit-cell parameters and resolution are given.

Crystallization conditions	Space group	Unit-cell angles (°)	Unit-cell dimensions (Å)	PDB code	Resolution (Å)
7% PEG 4000, 20–40 m*M* sodium (or potassium) citrate pH 5.6 or 6.5, 20–50 m*M* KNO_3 (in some cases) and 10% glycerol	*R*32	$\alpha = \beta = 90, \gamma = 120$	$a = b = 143.56, c = 519.64$	1oy6	3.68
			$a = b = 144.80, c = 518.61$	1oy8	3.63
			$a = b = 144.68, c = 517.51$	1oy9	3.80
			$a = b = 144.77, c = 517.89$	1oyd	3.80
			$a = b = 145.11, c = 517.16$	1oye	3.48
14% PEG 4000, 100 m*M* sodium phosphate pH 6.2 and 50 m*M* NaCl	*C*2	$\alpha = \gamma = 90, \beta = 97.71$	$a = 225.87, b = 134.42, c = 163.19$	2dhh	2.80
		$\alpha = \gamma = 90, \beta = 98.08$	$a = 227.05, b = 134.56, c = 161.70$	2dr6	3.30
		$\alpha = \gamma = 90, \beta = 98.17$	$a = 225.80, b = 134.47, c = 162.12$	2drd	3.10
8% PEG 4000, 50 m*M* ADA pH 6.5 and 200 m*M* $(NH_4)_2SO_4$	$P2_12_12_1$		$a = 146.18, b = 157.41, c = 246.04$	2j8s	2.54
12% PEG 4000, 0.1 *M* HEPES pH 7.5, 0.1 *M* NaCl and 0.3 *M* Li_2SO_4	*R*32	$\alpha = \beta = 90, \gamma = 120$	$a = b = 146.30, c = 514.30$	2i6w	3.10
8–10% PEG 3000, 40 m*M* potassium citrate pH 6.5 and 10% glycerol	*R*32	$\alpha = \beta = 90, \gamma = 120$	$a = b = 144.37, c = 518.93$	1t9t	3.23
			$a = b = 144.09, c = 518.80$	1t9u	3.11
			$a = b = 144.37, c = 518.44$	1t9v	3.80
			$a = b = 144.92, c = 516.67$	1t9y	3.64
			$a = b = 144.97, c = 519.37$	1t9x	3.08
			$a = b = 144.51, c = 519.36$	1t9w	3.23
6.5–8.5% PEG 3000, 30 m*M* sodium citrate pH 5.6 or 30 m*M* potassium citrate pH 6.5 and 8% glycerol	*R*32	$\alpha = \beta = 90, \gamma = 120$	$a = b = 145.40, c = 514.51$	2hqc	3.56
			$a = b = 145.04, c = 513.67$	2hqd	3.65
			$a = b = 145.65, c = 519.71$	2hqf	3.38
			$a = b = 144.90, c = 518.64$	2hqg	3.38
15–16% PEG 2000, 80 m*M* sodium phosphate pH 6.2, 20 m*M* sodium citrate–HCl pH 5.6	*R*32	$\alpha = \beta = 90, \gamma = 120$	$a = b = 144.54, c = 519.18$	1iwg	3.50
14–28% PEG 1000 or PEG 1500, 0.1 *M* Tris pH 7.5, 0.1 *M* Li_2SO_4, 18 m*M* *n*-octyl-β-D-thioglucopyranoside and 20% 1,2,3-heptanetriol	*R*32	$\alpha = \beta = 90, \gamma = 120$	$a = b = 145.10, c = 511.64$	2rdd	3.50
5% PEG 400, 16–22% PEG 300, 70 m*M* sodium citrate pH 4.6 and 8–11% glycerol	*C*2	$\alpha = \gamma = 90, \beta = 98.21$	$a = 222.80, b = 134.10, c = 161.01$	2gif	2.90
	*P*1	$\alpha = 103.9, \beta = 94.64, \gamma = 90.11$	$a = 127.33, b = 134.87, c = 140.84$	2hrt	3.00
31% PEG 400, 100 m*M* MES pH 6.6	*R*32	$\alpha = \beta = 90, \gamma = 120$	$a = b = 145.74, c = 514.00$	3d9b	3.42

meters as well as resolutions for all AcrB structures reported to date is shown in Table 3. The precipitating agent involved was PEG in all cases. Various buffers covering a wide pH range allowed *E. coli* AcrB crystal growth. The detergent used for crystallization was DDM in 23 of the 25 deposited structures (including this work). The two remaining structures were obtained with cyclohexyl-*n*-hexyl-β-D-maltoside (Cymal-6; Seeger *et al.*, 2006) as the crystallization detergent. Among these structures, 76% (19 of 25) were solved from rhombohedral crystals (*R*32) and always with similar unit-cell parameters. This provides a major criterion for the identification of AcrB rhombohedral crystals. To conclude, *E. coli* AcrB crystallizes under a variety of conditions and is probably not limited to those reported to date. Thus, this possible issue should always be kept in mind when crystallization screening is carried out for membrane proteins that have been heterologously overexpressed in *E. coli* and purified by IMAC.

3.4. Crystal-packing analysis

The molecular-replacement solution obtained from *MOLREP* was of good quality (R = 0.38). Typically, AcrB rhombohedral crystals contain one monomer in the asymmetric unit, with the functional AcrB trimer generated by the crystallographic threefold axis. The resulting AcrB structure is symmetric and comprises three conformationally identical monomers (Figs. 3*a* and 3*b*).

Examination of the crystal packing reveals that the AcrB trimers are arranged in a 'head-to-neck' manner (Fig. 4*a*). Each AcrB biological unit interacts with six equivalent trimers in the crystal lattice, three *via* their cytoplasmic regions and three *via* their periplasmic domains. We found some residual electron density at each interface between the cytoplasm-protruding regions of two AcrB trimers that corresponds to a unique nonprotein atom coordinated by four residues, two histidines and two aspartates, provided by the two adjacent trimers. As NaCl was the only salt added during purification, we assigned the atom as an Ni^{2+} ion from leakage of the affinity column used for purification. Indeed, the fortuitous assistance of such an Ni^{2+} ion in crystal packing has previously been observed in the case of the leukotriene C_4 synthase structure (Molina *et al.*, 2007). Interestingly, in our case this Ni^{2+} ion mediates a crystal contact between two AcrB trimers (Fig. 4*b*). The same residual electron density, confirmed by Fourier difference maps, is also present in some of the other deposited AcrB structures solved from rhombohedral crystals, but no assignment was reported. A multiple sequence alignment of nine AcrB homologues from different species reveals a high level of conservation of the two residues involved in metal binding (His525 and Asp529; Fig. 4*c*). Thus, if AcrB rhombohedral crystals were obtained from one of these homologues, a similar ion-mediated crystal contact might be expected. Nevertheless, the biological relevance of this metal-ion binding site is certainly low because its formation requires that two AcrB trimers from two different layers interact in a 'head-to-neck' manner and this is more than unlikely *in vivo*.

3.5. Comparison with other AcrB structures

The structure of AcrB solved in this study superimposes very well with previously published symmetric AcrB structures. The root-mean-square deviation (r.m.s.d.) between all matching main-chain atoms in our structure relative to PDB entry 2i6w (our molecular-replacement search model) and PDB entry 2rdd (the most recently solved AcrB symmetric structure) is 0.98 and 1.72 Å, respectively. Our symmetric AcrB structure is very similar to molecules *A* and *B* and significantly different from molecule *C* of the highest resolution asymmetric AcrB structure (PDB code 2j8s; data not shown). This is in agreement with previous observations (Sennhauser *et al.*, 2007).

In the RND superfamily the sequence of the N-terminus is highly conserved, with strict conservation of phenylalanine residues 4, 5 and 11 in several AcrB homologues (Das *et al.*, 2006). This sequence conservation points to a putative functional role for these three residues, which are located at the membrane–cytoplasm interface. Modelling of the six N-terminal residues has only been accomplished in two other symmetric AcrB structures. In one case (PDB code 2rdd) this region is in an α-helical conformation; in the second (PDB code 2i6w) it is in an extended conformation. The calculation of an OMIT map, removing the eight N-terminal residues, allowed us to build these residues in an α-helical conformation, as previously observed in PDB entry 2rdd and in most asymmetric AcrB structures. Consequently, unlike in PDB entry 2i6w, in our model the side chains of phenylalanine residues 4 and 5 are located in close proximity to phenylalanine residue 11 (Fig. 5). The involvement of this phenylalanine cluster in cytoplasmic substrate transport remains to be investigated.

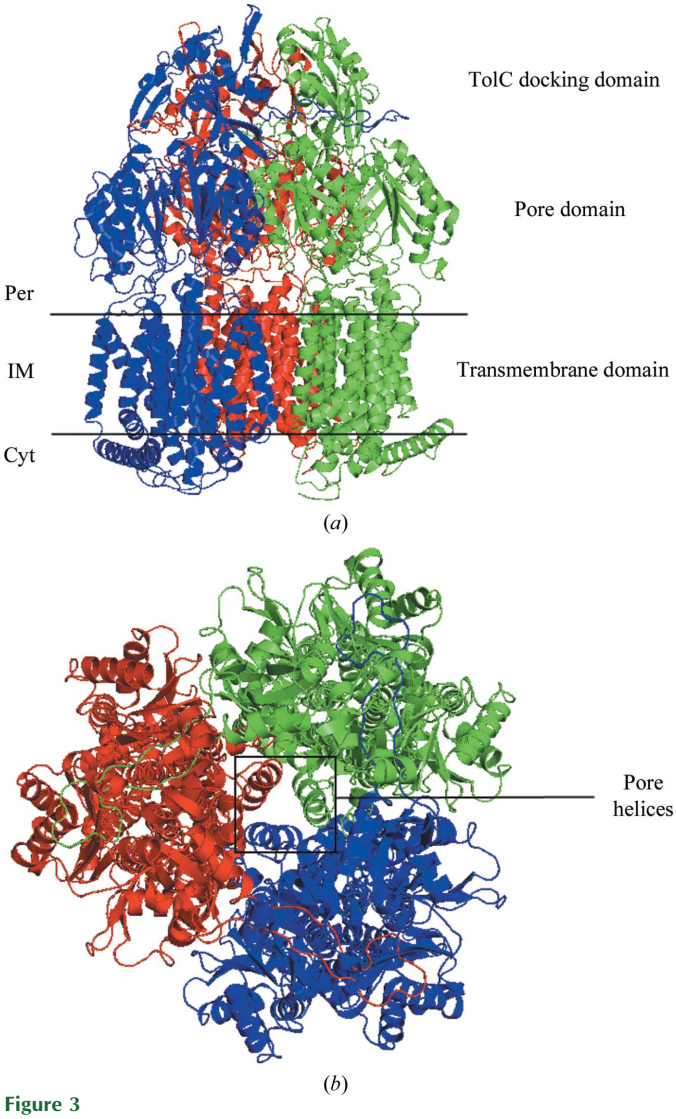

Figure 3
AcrB structure. (*a*) Side view of the AcrB trimer. The three protomers constituting the functional AcrB trimer are individually coloured (blue, red and green). The different domains are indicated. Per, periplasm; IM, inner membrane; Cyt, cytoplasm. (*b*) Periplasmic view of the AcrB trimer. The three central pore helices involved in the peristaltic pump mechanism (Murakami *et al.*, 2006; Seeger *et al.*, 2006; Sennhauser *et al.*, 2007) are indicated. Figs. 3–5 were created using *PyMOL* (DeLano, 2002).

4. Conclusions

The observation that *E. coli* AcrB spontaneously binds to IMAC resins was reported 9 y ago (Zgurskaya & Nikaido, 1999), but several European membrane-protein crystallography laboratories have recently encountered the problem of unintended AcrB crystallization (E-MeP members, personal communication). Furthermore, only two structures of endogenous *E. coli* AcrB have been deposited in the PDB (Das *et al.*, 2006; Törnroth-Horsefield *et al.*, 2007) and no report has made a clear critical analysis of this problem.

In the present case, it was not possible to detect AcrB contamination using classical Coomassie-stained SDS–PAGE. We estimated the AcrB concentration in our CorA purified sample to be about 0.1 mg ml^{-1}. This highlights the fact that AcrB can crystallize from very low concentrations and that it represents a major risk in membrane-protein crystallization when overexpression is carried out in *E. coli* and purification involves an IMAC step.

To avoid this problem, we propose either introducing a protease-cleavage site that allows removal of the His tag or using another affinity tag such as a Strep tag. Another elegant approach might be to use *E. coli* strains that are devoid of the *acrB* gene. A general

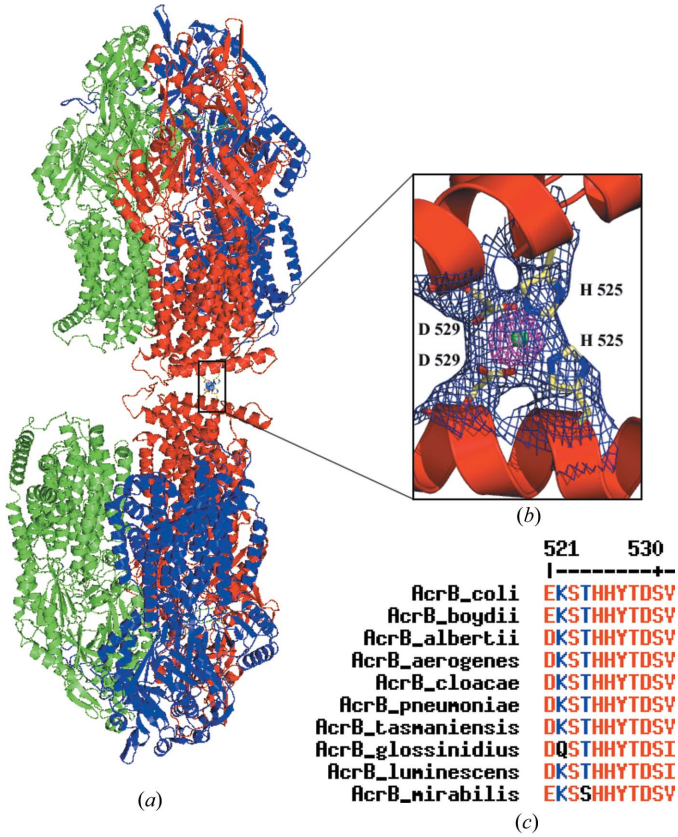

Figure 4
AcrB crystal packing. (*a*) AcrB 'head-to-neck' organization in the crystal lattice. The three protomers constituting each functional AcrB trimer are individually coloured (blue, red and green). (*b*) Enlargement of the Ni^{2+} ion-mediated crystal contact between two protomers from two different AcrB trimers. Residues His525 and Asp529 from each protomer are shown in stick representation and the Ni^{2+} ion is depicted as a green sphere. $2F_o - F_c$ electron density for these four residues and the Ni^{2+} ion is contoured at 1σ (blue) and 5σ (pink). (*c*) Multiple sequence alignment of AcrB homologues, revealing the very high degree of conservation for the residues binding the Ni^{2+} ion. Homologous AcrB sequences are from *Escherichia coli*, *Shigella boydii*, *Escherichia alberti*, *Enterobacter aerogenes*, *Enterobacter cloacea*, *Klebsiella pneumoniae*, *Erwinia tasmaniensis*, *Sodalis glossinidius*, *Photorhabdus luminescens* and *Proteus mirabillis*. The alignment was performed with *MULTIALIN* (Corpet, 1988).

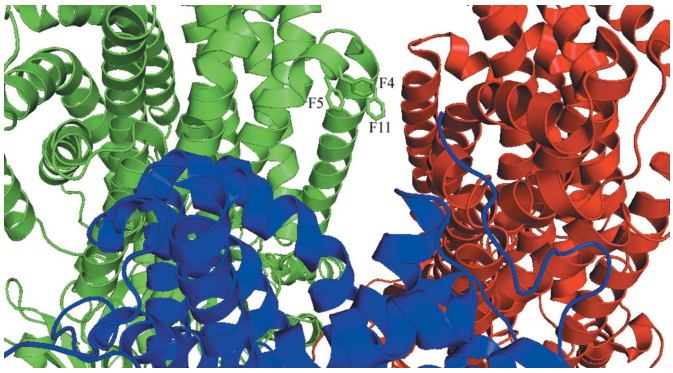

Figure 5
The three highly conserved phenylalanine residues at the N-terminus of AcrB. Phe4, Phe5 and Phe11 are shown in stick representations for one monomer. Each protomer is coloured individually (red, blue and green).

cautious approach would also be to check, when crystals are obtained, whether this combination of space group and unit-cell parameters are present in the PDB. Finally, an analysis of dissolved crystals should be performed by silver-stained SDS–PAGE and eventually by PMF–MALDI–TOF mass spectrometry.

This paper is the first to be dedicated to description of the AcrB contamination problem and of ways to avoid it. We also report for the first time an Ni^{2+} ion-mediated crystal contact in AcrB rhombohedral crystals.

We gratefully acknowledge fruitful discussions with the partners of the EU programme E-MeP as well as Professor Eric Chabrière. This work was funded in part by the EU E-MeP programme (FP6 Contract No. LSHG-CT2004-504601), by a Marie-Curie (AST-3D Contract No. MEIF-CT-2005-024761) grant to GS, by the Marseille-Nice Genopole and by a PhD grant from the 'Ministère Français de l'Enseignement Supérieur et de la Recherche' No. 22976-2006 to DV.

References

Brünger, A. T. (1992). *Nature (London)*, **355**, 472–475.
Cámara-Artigas, A., Hirasawa, M., Knaff, D. B., Wang, M. & Allen, J. P. (2006). *Acta Cryst.* F**62**, 1087–1092.
Collaborative Computational Project, Number 4 (1994). *Acta Cryst.* D**50**, 760–763.
Corpet, F. (1988). *Nucleic Acids Res.* **16**, 10881–10890.
Das, D., Xu, Q. S., Lee, J. Y., Ankoudinova, I., Huang, C., Lou, Y., DeGiovanni, A., Kim, R. & Kim, S. (2006). *J. Struct. Biol.* **158**, 494–502.
DeLano, W. L. (2002). *The PyMOL Molecular Graphics System.* http://www.pymol.org.
Emsley, P. & Cowtan, K. (2004). *Acta Cryst.* D**60**, 2126–2132.
Eshaghi, S., Niegowski, D., Kohl, A., Molina, D. M., Lesley, S. A. & Nordlund, P. (2006). *Science*, **313**, 354–357.
Hao, Q. (2001). *Acta Cryst.* D**57**, 1410–1414.
Helling, R. B., Janes, B. K., Kimball, H., Tran, T., Bundesmann, M., Check, P., Phelan, D. & Miller, C. (2002). *J. Bacteriol.* **184**, 3699–3703.
Kabsch, W. (1993). *J. Appl. Cryst.* **26**, 795–800.
Kehres, D. G. & Maguire, M. E. (2002). *Biometals*, **15**, 261–270.
Knoop, V., Groth-Malonek, M., Gebert, M., Eifler, K. & Weyand, K. (2005). *Mol. Genet. Genomics*, **274**, 205–216.
Lohkamp, B. & Dobritzsch, D. (2008). *Acta Cryst.* D**64**, 407–415.
Lunin, V. V., Dobrovetsky, E., Khutoreskaya, G., Zhang, R., Joachimiak, A., Doyle, D. A., Bochkarev, A., Maguire, M. E., Edwards, A. M. & Koth, C. M. (2006). *Nature (London)*, **440**, 833–837.
McCoy, A. J., Grosse-Kunstleve, R. W., Adams, P. D., Winn, M. D., Storoni, L. C. & Read, R. J. (2007). *J. Appl. Cryst.* **40**, 658–674.
Molina, D. M., Wetterholm, A., Kohl, A., McCarthy, A. A., Niegowski, D., Ohlson, E., Hammarberg, T., Eshaghi, S., Haeggström, J. Z. & Nordlund, P. (2007). *Nature (London)*, **448**, 613–617.
Murakami, S., Nakashima, R., Yamashita, E., Matsumoto, T. & Yamaguchi, A. (2006). *Nature (London)*, **443**, 173–179.
Murshudov, G. N., Vagin, A. A. & Dodson, E. J. (1997). *Acta Cryst.* D**53**, 240–255.
Painter, J. & Merritt, E. A. (2006). *Acta Cryst.* D**62**, 439–450.
Payandeh, J., Canhui, L., Ramjeesingh, M., Poduch, E., Bear, C. E. & Pai, E. F. (2008). *J. Biol. Chem.* **283**, 11721–11733.
Payandeh, J. & Pai, E. F. (2006). *EMBO J.* **25**, 3762–3773.
Seeger, M. A., Schiefner, A., Eicher, T., Verrey, F., Diederichs, K. & Pos, K. M. (2006). *Science*, **313**, 1295–1298.
Sennhauser, G., Amstutz, P., Briand, C., Storchenegger, O. & Grütter, M. G. (2007). *PLoS Biol.* **5**, 106–113.
Shevchenko, A., Wilm, M., Vorm, O. & Mann, M. (1996). *Anal. Chem.* **68**, 850–858.
Suhre, K. & Sanejouand, Y.-H. (2004). *Acta Cryst.* D**60**, 796–799.
Törnroth-Horsefield, S., Gourdon, P., Horsefield, R., Brive, L., Yamamoto, N., Mori, H., Snijder, N. & Neutze, R. (2007). *Structure*, **12**, 1663–1673.
Vagin, A. & Teplyakov, A. (1997). *J. Appl. Cryst.* **30**, 1022–1025.
Xu, B., Jahic, M. & Enfors, S. (1999). *Biotechnol. Prog.* **15**, 81–90.
Zgurskaya, H. I. & Nikaido, H. (1999). *Proc. Natl Acad. Sci. USA*, **96**, 7190–7196.